



HAL
open science

Ability of the R3 test to evaluate differences in early age reactivity of 16 industrial ground granulated blast furnace slags (GGBS)

Simon Blotevogel, Andreas Ehrenberg, Laurent Steger, Lola Doussang, Judit Kaknics, Cédric Patapy, Martin Cyr

► To cite this version:

Simon Blotevogel, Andreas Ehrenberg, Laurent Steger, Lola Doussang, Judit Kaknics, et al.. Ability of the R3 test to evaluate differences in early age reactivity of 16 industrial ground granulated blast furnace slags (GGBS). *Cement and Concrete Research*, 2020, 130, pp.105998. 10.1016/j.cemconres.2020.105998 . hal-02501098

HAL Id: hal-02501098

<https://hal.science/hal-02501098>

Submitted on 26 Jun 2020

HAL is a multi-disciplinary open access archive for the deposit and dissemination of scientific research documents, whether they are published or not. The documents may come from teaching and research institutions in France or abroad, or from public or private research centers.

L'archive ouverte pluridisciplinaire **HAL**, est destinée au dépôt et à la diffusion de documents scientifiques de niveau recherche, publiés ou non, émanant des établissements d'enseignement et de recherche français ou étrangers, des laboratoires publics ou privés.

1 **Ability of the R3 test to evaluate differences in early age reactivity of 16**
2 **industrial ground granulated blast furnace slags (GGBS)**

3 Postprint version of the article published in Cement and Concrete Research under DOI:
4 10.1016/j.cemconres.2020.105998

5 **Authors**

6 Simon Blotevogel¹, Andreas Ehrenberg², Laurent Steger^{1,3}, Lola Doussang³, Judit Kaknics⁴, Cedric
7 Patapy¹, Martin Cyr¹

8 ¹LMDC, Université de Toulouse, INSA/UPS Génie Civil, 135 Avenue de Rangueil, 31077, Toulouse
9 cedex 04, France

10 ²Institut Für Baustoff-Forschung EV (FEHS), Bliersheimer Str.62, Duisburg 47229, Germany

11 ³Ecocem Materials, 324061, Block F1, Eastpoint Business Park, Dublin 3, Ireland

12 ⁴ArcelorMittal Maizieres Research, Voie Romaine, 57283 Maizières-les-Metz, France

13

14 **Abstract**

15 Ground granulated blast furnace slag (GGBS) is a glassy by-product of pig iron production and is
16 commonly used in concrete industry to replace cement and thereby lower the carbon footprint of
17 the material. Large variations in reactivity exist depending on the GGBS physical and chemical
18 features. Here we investigate the ability of three rapid calorimetric methods to evaluate the
19 reactivity of GGBS. On a set of 16 industrial GGBS, we show that 24h heat release, using the R3-
20 protocol, correlates well with 2d compressive strength of standard mortars using 75 wt.-% GGBS. The
21 correlation of R3-test results ($R^2= 0.87$) is better than for traditional reactivity indices calculated from
22 chemical composition. Furthermore, we present data on the repeatability of the test protocol and
23 show that the R3 protocol is very sensitive to sample fineness. Finally, XRD patterns show that slight
24 differences in phase assemblage exist between the most and least reactive GGBS.

25 **1. Introduction**

26 Ground granulated blast furnace slag (GGBS) is a glassy by-product of pig iron production and has
27 been used in blended cements for over 140 years [1]. Besides economic aspects the use of GGBS at
28 high substitution levels has the advantage of lowering CO₂ footprint of concrete, decreasing heat
29 development during setting and increasing physical and chemical resistance of the material [1–6].
30 However, short term compressive strength development of GGBS is below that of original Portland
31 cement (OPC), but reactivity under same conditions, can differ widely between different GGBS
32 [1,4,7–10].

33 The intrinsic reactivity of GGBS depends on different parameters as chemical composition, glass
34 content and structure or quenching parameters of the slag [1,9,11–13]. This makes modification of
35 production parameters of GGBS – so called upstream modification - a promising route to increase its
36 reactivity [13–15]. Another way to increase the reactivity of GGBS is the modification of the
37 activation system (downstream) by increasing fineness, increasing reaction temperature, adapting
38 solution chemistry or by adding chemical activators as CaCl₂ [16–18].

39 The present work originates in the European research project Actislag, aiming to develop a second
40 generation GGBS reaching cement substitution rates of 80 wt.-% while keeping the specifications of
41 CEM II. Therefore, both activation routes are considered: upstream modifications of GGBS
42 chemistry/microstructure and downstream modifications of the activation system. In order to reach
43 the research goals, it is essential to be able to quickly assess the reactivity of a large number of GGBS.
44 Furthermore, as upstream modifications will be tested in lab scale trials, minimal sample mass should
45 be used for the reactivity tests.

46 A multitude of test methods are available to predict the reactivity of supplementary cementitious
47 materials (SCM). Usually chemical tests are used to predict short term compressive strength, see
48 Snellings and Scrivener (2016) and Li et al. (2018) for a review [19,20]. Standardized test methods use

49 Ca consumption during hydration of the SCM (e.g. Chapelle test, Frattini test). These were designed
50 for pozzolanic material and are difficult to apply to slags, as GGBS contain a substantial amount of
51 reactive Ca [19]. Further methods aim to determine the degree of reaction of SCMs: most notably
52 selective dissolution, SEM-IA, XRD, and NMR (27-Al or 29-Si) are presented in scientific literature but
53 are often time consuming and with moderate accuracy at early age [21].

54 In recent publications heat development during hydration of a simplified system showed good
55 correlation with compressive strength of different SCM containing mortars [19,20,22]. In these
56 studies, a sulphate containing alkaline solution is added to a mix of portlandite, carbonates and the
57 respective SCM. The heat development during the following reaction is measured by isothermal
58 calorimetry. The reaction can be accelerated by increasing the temperature conditions. This setup
59 avoids the use of other hydraulic material as OPC, and thus the risk of overprinting the signal of
60 intrinsic SCM reactivity [23–25]. By this protocol a wide range of SCMs including GGBS, fly ash,
61 natural pozzolans and calcined clays were tested and classified according to their reactivity. In Avet
62 et al. (2016) the simplified test was used to predict the pozzolanic activity of 7 calcined clays, naming
63 it R3 test [22]. In that study a good prediction of compressive strength of mortars containing 30 wt.-
64 % calcined clays was obtained after 1d of calorimetric measurement at 40°C for all setting ages. Li et
65 al. 2018 reached a good prediction of 28d compressive strength of mortars at a replacement rate of
66 30 wt.-% of cement by different SCMs. They used the same calorimetric test, but the best correlation
67 between 28d compressive strength and heat development was reach for 3 and 7 d of calorimetric
68 measures. Other studies used a similar test design to determine hydraulic or pozzolanic properties of
69 different materials, including GGBS [26–28]. However, it was never attempted to use the R3 test to
70 rank different GGBS according to their early age reactivity.

71 Another promising method to judge GGBS reactivity in literature is proposed by Kashani et al. (2014)
72 [29]. In this study pure 1 molar NaOH is used as activation system which gives exploitable results in

73 less than 12 h in ambient temperature isothermal calorimetry, nevertheless no comparison between
74 different GGBS was attempted.

75 In the present study, 16 industrial GGBS from different sources were examined in terms of
76 composition and mechanical performance in binder pastes. Subsequently different calorimetric
77 protocols existing in literature were tested in order to develop a rapid and reliable method using
78 minimal sample mass to evaluate GGBS short term performance in cementitious systems. The three
79 main objectives of this study are:

- 80 1. Evaluation of existing calorimetric tests for the assessment of young age compressive
81 strength of GGBS. Main focus is on protocols based on the R3 test and the optimization of
82 grinding parameters.
- 83 2. Application of an optimized calorimetric test on a set of 16 industrial slags and comparison of
84 test results with actual compressive strength values in order to evaluate the capacity of the
85 test to evaluate the reactivity of different GGBS.
- 86 3. Discussion of sources of differences in reactivity of the analyzed GGBS, especially chemical
87 composition of the slags and mineral phases formed during the calorimetric test.

88

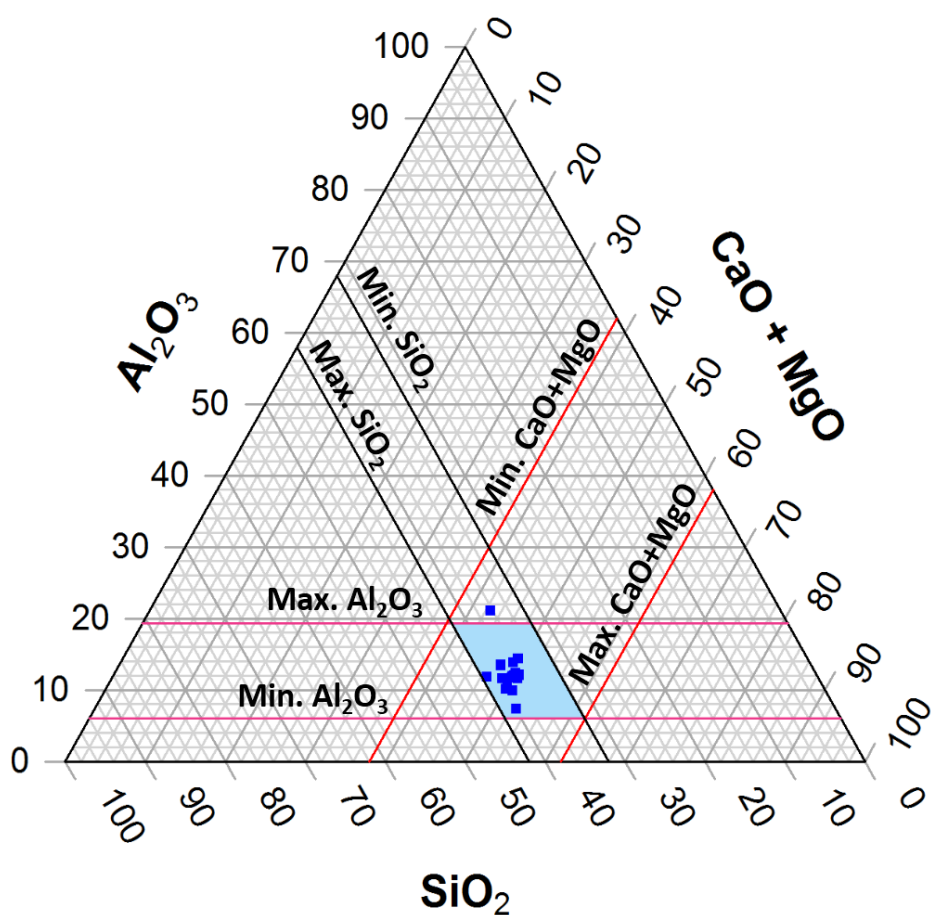
2. Materials

2.1 Chemical composition of industrial GGBS

91 In order to represent a wide range of today's GGBS compositions, 16 different slags were selected
92 from the FEhS database (FEhS – Institut für Baustoff-Forschung e.V., Duisburg, Germany). Chemical
93 composition was measured on fused tabs by XRF (Panalytical Zetium). The composition was
94 calculated conventionally as oxides (Table 1). Major element compositions and maximum values
95 from literature are displayed in Figure 1. CaO contents in our dataset are between 29.0 and 43.2 wt.-
96 %. The lowest value is lower than lowest values reported in literature, but the highest value is also
97 4.3 wt.-% lower than maxima reported [1]. Most GGBS contain between 40 and 42 wt.-% CaO. SiO₂
98 contents in our GGBS set range from 34.6 to 39.2 wt.-%, a distribution that is on both ends about 2 %
99 smaller than the extreme values for GGBS from different regions of the world reported in Matthes et
100 al. (2018) [1]. For Al₂O₃ the observed concentrations range between 6.8 to 20.1 wt.-%, which
101 corresponds to extreme values reported in literature [1]. However, only GGBS 15 attains such a high
102 Al₂O₃ content (20.1 wt.-%), the next lower sample (GGBS 14) contains 13.7 wt.-% Al₂O₃. The majority
103 of selected GGBS contain between 10 and 12 wt.-% Al₂O₃. MgO contents in our sample set are
104 between 6.12 and 11.6 wt.-%, both extrema are 3 % below extreme values reported by Matthes et al
105 (2018) [1]. In the studied GGBS, TiO₂ contents range for 0.27 to 3.02 wt.-%. With 3.02 wt.-% of TiO₂ in
106 GGBS 9 the extreme values again correspond to the values observed by Matthes et al. (2018) [1]. In
107 contrast, most GGBS contain between 0.5 and 1 wt.-% TiO₂. Reactivity indices were calculated
108 according to the composition data.

109 Glass content of the 16 GGBS was measured by optical transmission light microscopy at FEhS. The
110 sample was ground in an agate mortar and the 40-63 µm fraction was embedded in Canada balm.
111 Then, glass content (in vol.-%) was measured on individual grains, using a lambda plate and
112 polarisators 1000. The method is described in detail in Drissen (1994) [30]. Glass content of all slags
113 was >99.8 vol.-%, only exceptions were GGBS 14 (98.2 vol.-%) and GGBS 15 (94.5 vol.-%).

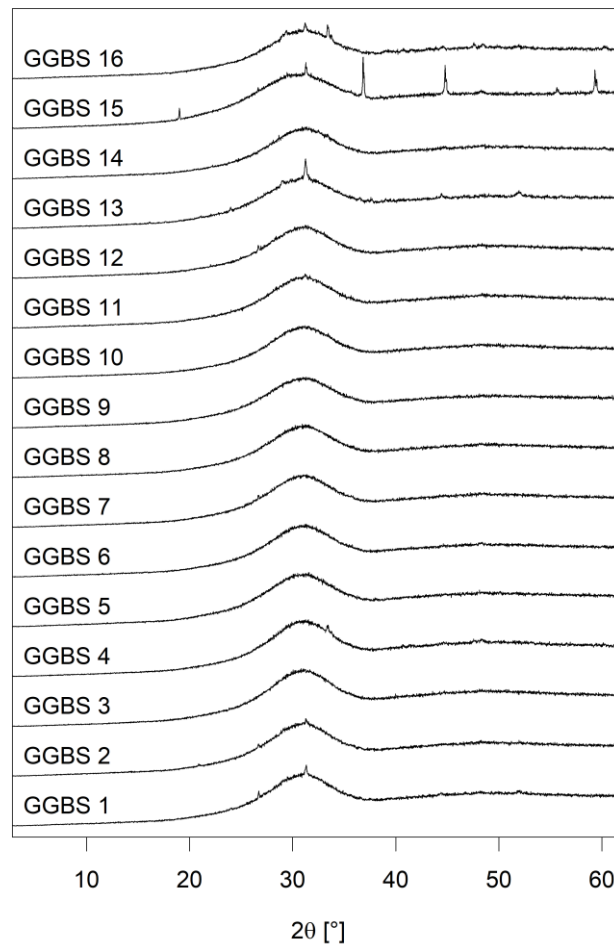
114 Furthermore, XRD scans were performed on the unhydrated slags (Figure 2). The measurement
115 parameters were the same as described in section 3.3. Rietveld refinement using rutile as external
116 standard gave an amorphous content of 96.2 vol.-% and 3.8 vol.-% of Spinel in GGBS 15. This is well
117 in line with glass content measurements. In GGBS 13, amorphous content 97.4 vol.-% and 2.6 vol.-%
118 of akermanite were modelled, slightly more than expected from glass content measurements. In all
119 other samples, the crystalline signal was too weak to be modelled by Rietveld refinement, in line with
120 glass content measurements. However, traces of merwinite were detected in GGBS 4 and GGBS 16,
121 and traces of akermanite in GGBS 1, GGBS 2, GGBS 11 and GGBS 16.



122
123 **Figure 1. Major chemical composition of the 16 slags used in this study. The sum of concentration**
124 **of the four presented elements was normalized to 100 wt.--%. Lines indicate minimum and**

125 maximum contents reported in Matthes et al. (2018) [1]. The blue patch indicates possible range of
126 composition within those limits.

127



128

129 **Figure 2. XRD scans of unhydrated GGBS. All GGBS have a high amorphous content. Crystalline phases were**
130 **modelled for GGBS 15 and GGBS 13 using Rietveld refinement. GGBS 15 contains 3.8 vol.-% spinel and GGBS**
131 **13 2.6 vol.-% akermanite. For all other slags crystalline signal was too low to be modelled. However, traces of**
132 **merwinite and/or akermanite were detected in GGBS 1, GGBS 2, GGBS 4, GGBS 11, GGBS 16.**

133 **Table 1. GGBS compositions as determined by XRF. Mean values and relative standard deviation**
134 **(RSD, in %) are given for the measured parameters.**

135

ID	CaO wt.-%	SiO ₂ wt.-%	Al ₂ O ₃ wt.-%	MgO wt.-%	TiO ₂ wt.-%
GGBS 1	41.4	36.4	13.6	6.80	0.75
GGBS 2	42.0	36.6	12.0	6.94	0.74
GGBS 3	40.9	37.6	9.61	6.40	0.61
GGBS 4	42.1	37.0	9.41	6.12	0.66
GGBS 5	38.4	37.1	12.9	7.32	0.77
GGBS 6	41.2	35.6	11.0	6.84	1.79
GGBS 7	41.7	36.7	11.5	6.35	0.70
GGBS 8	40.9	36.6	11.2	6.84	1.12
GGBS 9	39.5	37.4	11.0	6.64	3.02
GGBS 10	41.7	38.0	10.1	6.46	0.40
GGBS 11	43.2	36.3	11.8	6.30	0.43
GGBS 12	42.0	36.8	11.7	6.60	0.70
GGBS 13	33.9	39.2	11.2	10.4	0.57
GGBS 14	38.9	34.6	13.7	8.36	1.16
GGBS 15	29.0	34.6	20.1	11.6	0.78
GGBS 16	37.4	36.7	6.8	11.1	0.27
Mean	39.6	36.7	11.7	7.6	0.90
RSD (%)	9.2	3.1	23.9	23.9	73.8

136

137 **2.2 Other Materials**

138 The chemical composition of the clinker used for compressive strength tests is reported in Table 2.

139 XRD analysis followed by Rietveld refinement gave a mineral composition of 60.9 wt.-% C3S, 21.5 wt.-%

140 % C2S, 0.9 wt.-% orthorhombic C3A, 7.8 wt.-% cubic C3A and 6.6 wt.-%C4AF. Density was 3.093

141 g/cm³ and fineness 4200 cm²/g (Blaine). Further reactants used were K₂SO₄ (VWR, REACTAPUR), KOH

142 (VWR, AnalaR Normapur), Ca(OH)₂ (Merck, ACS Reagent, for analysis). Water used for calorimetric

143 tests was always pure (18.2MΩ).

144

145 **Table 2. Composition of the clinker used for compressive strength test and calorimetric tests. The**
146 **values were determined by XRF.**

Component	Content
	wt.-%
CaO	66.20
Free lime	0.64
MgO	1.00
SiO ₂	22.10
Al ₂ O ₃	5.20
Fe ₂ O ₃	2.30
Mn ₂ O ₃	<0.05
Cr ₂ O ₃	<0.05
TiO ₂	0.30
Na ₂ O	0.20
K ₂ O	0.74
S total	0.39
CO ₂	0.07
H ₂ O	0.17

147

148

149 **3. Methods**

150 **3.1 Compressive strength tests**

151 Mortar strength tests according to EN 196-1 were performed in order to evaluate reactivity of GGBS
152 [31]. A batch of 5 kg of each GGBS was ground in a ball mill using a mixture of steel spheres and
153 cylinders. To achieve a fineness of about 4200 cm²/g according to EN 196-6, the grinding time was
154 about 3 hours [32]. However, the decisive parameter to evaluate the achieved fineness was the
155 particle size distribution measured by laser diffraction granulometry (Horiba LA 300). Based on a
156 weighted double logarithmic transformation according to the RRSB method, the PSD parameters d'
157 (d_{63.2%}) and n (slope) were calculated. For each sample, 6 standard prisms (4 x 4 x 16 cm³) were made
158 using 75 wt.-% of GGBS and 25 wt.-% of clinker according to EN 196-1, subsequently adding 4.5 wt.-%
159 of SO₃, in form of a mixture of 25 wt.-% gypsum and 75 wt.-% anhydrite. A water binder ratio of 0.5
160 was used. Compressive strength tests were performed after 1d, 2d, 7d, 28d and 91d storing times at
161 20°C under water.

162 **3.2 Isothermal Calorimetry**

163 All calorimetric tests were carried out using a TAM Air isothermal calorimeter by TA-instruments.
164 Samples were prepared in 10 mL polypropylene recipients. The pastes were hand stirred using a glass
165 bar until no agglomerates or layering was visible anymore. Only exception was the 7d calorimetric
166 test using clinker, based on EN196-9, for which samples were prepared in a 20 mL admixture cell
167 [33]. Results of calorimetric measurements were normalized to GGBS mass in the vessel.

168 **3.3 Characterization of hydrated phases**

169 Hydrates were characterized directly after the calorimetric measurements. The hydrated slag sample
170 was crushed in an agate mortar and the resulting powder was briefly suspended in a stirred beaker
171 containing isopropanol to remove remaining water. The powder was then recovered through vacuum
172 filtration and the sample was rinsed with acetone three times. Finally, the dry powder retained by

173 the filter was directly used for XRD analysis on a Bruker D8 using a Cu-cathode. Scan duration was
 174 65 min for angles from 2 to 70°. The sample preparation from calorimeter to the start of XRD scan
 175 took less than 1h.

176 3.4 Method adaption for estimation of slag reactivity

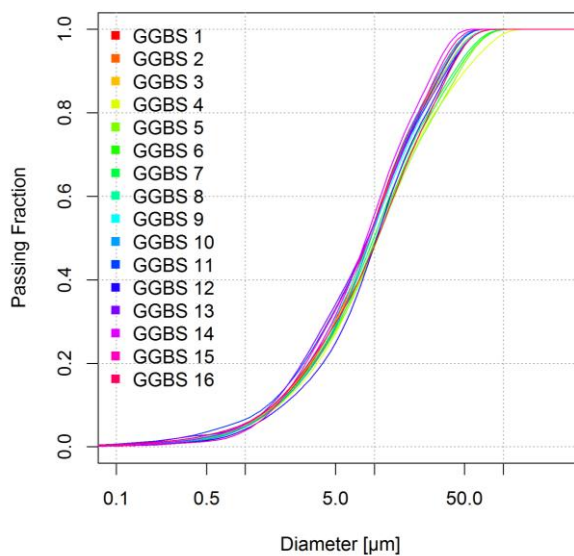
177 In a first step, three modified, rapid test protocols from literature, described in Table 3, were tested
 178 for their capacity to predict compressive strength of slag-based mortars. The R3 protocol was
 179 modified in the sense that no calcite addition was used and the test proposed in Snellings and
 180 Scrivener 2016 was modified by reducing the amount of Ca(OH)₂ and not adding sulfates to the mix
 181 [19,20,22]. Therefore, six GGBS, covering a wide range of reactivity, were selected. Furthermore,
 182 heat development under the same conditions as the compressive strength tests (adding 25 wt.-%
 183 clinker, and anhydrite/gypsum to reach 4.5 wt.-% SO₃) was measured. For these tests, the same
 184 grinding protocol as for compressive strength tests was used.

185 **Table 3. Summary rapid calorimetric tests take from literature and the standard test imitating**
 186 **conditions of the compressive strength measurements. Protocols were slightly modified to suit the**
 187 **needs of this study.**

Protocol based on	liquid/solid ratio	Solid additions	Activation solution	Temperature	Duration
Kashani et al. 2014	0.45	-	0.5 M NaOH	20°C	20h
Avet et al. 2016 and Li et al. 2018. R3-Test	1.25	Ca(OH) ₂ (3:1) (addition : slag)	0.3 M K from KOH + K ₂ SO ₄ (1 : 5 w/w)	40°C	24h
Snellings and Scrivener 2016	0.83	Ca(OH) ₂ (2:1)	0.5 M KOH	40°C	24h
FEhS database for GGBS (75 wt.-% GGBS, 25 wt.-% CL [34])	0.50	Clinker/GGBS (1:3) 4.5 wt.-% SO ₃	H ₂ O	20°C	7d

188

189 Next, the repeatability of the R3 protocol was tested measuring 7 times the same powder (GGBS 11)
 190 to calculate errors associated with the calorimetric method. Subsequently, the same granulate (GGBS
 191 14) was ground six times and analyzed with the modified R3 test. Therefore, the samples were
 192 ground using a Retsch RS100 disc mill. 15 g of each GGBS was put in a 50 mL tungsten carbide bowl
 193 for 1 minute at 1400 rpm to a Blaine fineness of 4100 ± 100 cm²/g [32].



194

195 **Figure 3. Granulometric curves of 16 ground industrial GGBS samples, after applying the same**
 196 **grinding protocol.**

197 As the repeatability of the whole protocol was judged sufficient, the grinding process and the R3
 198 calorimetric measurements were applied to the set of 16 industrial GGBS. The particle size
 199 distribution was measured on a CILAS 1090 laser diffraction granulometer operating with ethanol to
 200 check repeatability of the grinding protocol (Figure 3). Three successive measurements in Fraunhofer
 201 mode were carried out on each powder sample. Samples received 3x30 s ultrasonic treatment before
 202 measurement in order to avoid agglomerations. The PSD analysis gave d_{10} values between 1.6 and
 203 1.8 μm and d_{50} values between 8.5 and 10.5 μm . These values were judged sufficiently close to
 204 exclude a major influence of sample finesse.

205 In addition, 50 g of GGBS 2 and GGBS 14 samples were ground for 2x30 s, 3x30 s, 4x30 s and 5x30 s in
 206 the 250 mL bowl described above, in order to be able to quantify the impact of fineness on
 207 calorimetric measurements.

208

209

4. Results

4.1 Chemical and mechanical analysis of GGBS

210 Mean compressive strength values are 2.8, 9.9, 30.7, 44.8 and 53.9 MPa at 1 d, 2 d, 7 d, 28 d and 91
211 d, respectively (Table 4). Measured compressive strength values logically increase with time for all
212 samples. Compressive strength after 1 d is between 2.0 MPa in GGBS 9, the sample with the highest
213 TiO_2 content, and 3.9 MPa in GGBS 2 and GGBS 11. This means a relative difference of almost a factor
214 2 in mechanical performance between different slags. Note that no compressive strength
215 measurements are available for GGBS 15 and GGBS 16 at this age. After 2 d, measured values range
216 from 3.7 (GGBS 16) to 17.1 MPa (GGBS 15), making up for difference of more than a factor 4
217 between the least and most reactive slag. These two are also the samples with the respectively
218 lowest and highest Al_2O_3 contents (Table 1). The relative standard deviation (RSD) of compressive
219 strength tests between samples increases to 38.4 % at 2 d time. RSD between samples then
220 decreases over time (24.2 % after 7d and 14.3 % after 28 d) and is as low as 12.5 % after 91 d.

222 After 7 d, 28 d and 91 d time, GGBS 11 developed highest compressive strength (40.0, 54.3 and 62.4
223 MPa, respectively), this is also the sample with the highest CaO content (Table 1). This slag was
224 already the most effective after 1 d when no data for GGBS 15 was available, but overtaken by GGBS
225 15 at 2 d. The relative performance of GGBS 15, the sample with the highest Al_2O_3 content and the
226 lowest CaO content decreased over time. GGBS 16 continued to be the least reactive slag (12.0, 26.5
227 and 32.7 MPa, respectively). Note that the relative difference between the most and least reactive
228 GGBS decreased at later ages. Between the extreme values, several slags interchanged their ranks at
229 7d, 28 d and 91 d, so that no clear tendency was visible. At 91 d all GGBS have reached compressive
230 strength values of >50 MPa, with only two exceptions (GGBS 15 and GGBS 16).

231

232

233 **Table 4. Results of compressive strength tests on mortar (75 wt.-% GGBS: 25 wt.-% Clinker). Mean**
 234 **values and relative standard deviation (RSD, in %) of 6 mortar bar specimens are given for all**
 235 **parameters.**

ID	1 d	2 d	7 d	28 d	91 d
	MPa	MPa	MPa	MPa	MPa
GGBS 1	3.1	11.0	33.8	44.6	55.3
GGBS 2	3.9	11.2	37.3	47.5	56.7
GGBS 3	2.6	8.2	32.3	48.5	55.6
GGBS 4	2.8	9.4	32.4	48.9	57.3
GGBS 5	2.7	9.2	32.2	45.5	55.6
GGBS 6	2.4	9.2	28.1	45.5	54.9
GGBS 7	2.8	11.2	34.8	44.4	54.9
GGBS 8	2.1	10.3	31.4	43.8	51.8
GGBS 9	2.0	4.3	18.0	37.9	53.6
GGBS 10	2.5	7.4	32.7	46.3	51.2
GGBS 11	3.9	15.6	40.0	54.3	62.4
GGBS 12	3.1	10.6	39.2	50.6	57.7
GGBS 13	2.2	5.1	23.4	44.6	57.2
GGBS 14	3.0	14.8	35.1	49.2	59.4
GGBS 15	-	17.1	29.3	38.2	46.1
GGBS 16	-	3.7	12.0	26.5	32.7
Mean	2.8	9.9	30.7	44.8	53.9
RSD (%)	20.9	38.4	24.2	14.3	12.5

236 **4.2 Reactivity indices**

237 Reactivity indices are routinely used to evaluate GGBS quality. For the set of 16 industrial GGBS,
 238 different reactivity indices were calculated based on oxide contents of GGBS (Table 1), using formulas
 239 commonly found in literature (see Matthes et al., 2018, for discussion and initial sources [1]). Only
 240 the F-value by Ehrenberg (2015) was added [35]. Correlation coefficients (Pearson's R^2) between
 241 index values and measured compressive strength are given in Table 5. Most reactivity indices do not
 242 explain more than a third of the variance ($R^2 < 0.33$) observed in actual compressive strength
 243 measurements. Only the German standard for special cement, the basicity by Schwiете, the F-value
 244 by Keil and the F-value by Ehrenberg explain higher proportions of variance in compressive strength
 245 tests at some ages. Strongest correlations are found for 2 d compressive strength for the F-value by
 246 Keil ($R^2=0.71$), and Ehrenberg ($R^2=0.71$) and the German standard for special cement ($R^2=0.78$). At

247 younger and older ages, correlations are less well defined. Only the basicity by Schwiete gives
 248 stronger correlations at 7d ($R^2=0.63$) then after 2d ($R^2=0.51$). The Schwiete basicity never drops
 249 below a correlation coefficient of 0.33 with R^2 of 0.41, 0.39 and 0.33 for 1 d, 28 d and 91 d,
 250 respectively. The Keil F-value also correlates well to 7 d compressive strength ($R^2=0.43$) but for all
 251 other ages drops below $R^2 = 0.33$. The F-value according to Ehrenberg correlates well with 1 d and 7 d
 252 strength (R^2 of 0.56 and 0.66 respectively) and the German standard for special cement only
 253 correlates with 1 d compressive strength ($R^2=0.37$).

254 **Table 5. Pearson's R^2 of correlation between compressive strength at different mortar ages and**
 255 **reactivity coefficients calculated based on GGBS composition. Linear regression was carried out on**
 256 **all 16 GGBS characterized in this study except for the age of 1 d where the 14 first slags were used.**
 257 **Reactivity indices are taken from Ehrenberg (2015) and Matthes et al., (2018), original sources are**
 258 **cited therein [1,35].**

Reactivity index	Definition	1 d	2 d	7 d	28 d	91 d
Basicity according to Tetmajer	$\frac{C}{S}$	0.30	0.02	0.27	0.26	0.18
European Standard for slag cement (1994)	$\frac{(C + M)}{S}$	0.32	0.11	0.15	0.09	0.04
German Standard for special cement (1942)	$\frac{(C + M + A)}{S}$	0.37	0.78	0.31	0.08	0.05
German Standard for Eisenportlandzement (1909)	$\frac{(C + M)}{(S + A)}$	0.15	0.13	0.00	0.00	0.01
German Standard for Hochofenzement (1932)	$\frac{(C + M + \frac{1}{3}A)}{(S + \frac{2}{3}A)}$	0.29	0.01	0.03	0.02	0.00
Basicity by Schwiete	$\frac{(C + A - 10)}{(S + 10)}$	0.41	0.51	0.63	0.39	0.33
F-Value according to Keil (1942)	$\frac{(C + \frac{1}{2}M + \frac{1}{2}S^{2-} + A)}{(S + MnO)}$	0.36	0.65	0.48	0.21	0.16

F-Value according Ehrenberg (2015)	$\frac{(C + \frac{1}{2}M + \frac{1}{2}S^{2-} + A)}{(S + MnO + (TiO_2)^2)}$	0.56	0.71	0.66	0.26	0.09
------------------------------------	--	------	------	------	------	------

259

260 4.3 Correlating heat of hydration to compressive strength

261 4.3.1 Choice of the method

262 The results of heat measurement of 6 selected slags using different methods are reported in Table 6.
 263 Note that heat values are normalized to slag mass in the measurement vessel. For all three rapid test
 264 methods the ranking of samples by heat development is similar. GGBS 13 is developing the least heat
 265 whereas GGBS 14 shows the most exothermic reaction. Only in the method by Kashani et al. (2014),
 266 without Ca addition, the lowest heat development is measured in GGBS 3 [29]. The methods taken
 267 from Snellings and Scrivener (2016) and the R3 test gave the same ranking and similar magnitudes of
 268 heat development [19,20,22]. However, the range of measured values is slightly larger in the R3-test
 269 (between 187 and 303 J/g) than in the protocol taken from Snellings and Scrivener (between 184 and
 270 257 J/g). Divided by their respective mean heat values this gives a relative span of 47 % for the R3
 271 test and 31 % for the Scrivener and Snellings (2016) protocol, showing that the R3-test has a better
 272 discriminatory capacity. Heat development per mass GGBS is lowest in the teste taken from Kashani
 273 et al. (2014). The range of the measured values between 35.5 and 43.8 J/g is low, even considering
 274 the low average heat of 40.1 J/g (relative span, 21 % of the mean). In the method imitating
 275 compressive strength test by clinker addition, GGBS 11 has the highest heat development and GGBS
 276 13 the least. The range of the data relatively close, between 308 and 366 J/g for an average of 335
 277 J/g (17 % of the mean), giving the test lowest discriminatory capacity of the four tested methods.

278

279

280

281

282 **Table 6. Heat development of six selected slags measured by different protocols together with**
 283 **Pearson’s R² of linear regressions between heat and compressive strength for various curing times.**
 284 **Heat values are normalized to slag mass in the vessel.**

Kashani et al. 2014		Modified Snellings and Scrivener 2016		R3, Avet et al. 2016, Li et al. 2018		7 d using clinker as compressive strength test	
Slag ID	Heat 20h [J/g]	Slag ID	Heat 24h [J/g]	Slag ID	Heat 24h [J/g]	Slag ID	Heat 7d [J/g]
GGBS 2	42.8	GGBS 2	240	GGBS 2	246	GGBS 2	337
GGBS 3	35.5	GGBS 3	218	GGBS 3	220	GGBS 3	340
GGBS 11	42.4	GGBS 11	250	GGBS 11	287	GGBS 11	366
GGBS 12	39.1	GGBS 12	230	GGBS 12	232	GGBS 12	322
GGBS 13	37.5	GGBS 13	184	GGBS 13	187	GGBS 13	308
GGBS 14	43.2	GGBS 14	257	GGBS 14	303	GGBS 14	335

R² for linear regression between compressive strength and heat of hydration

1 d	0.58	1 d	0.58	1 d	0.40	1 d	0.53
2 d	0.67	2 d	0.92	2 d	0.95	2 d	0.59
7 d	0.34	7 d	0.73	7 d	0.47	7 d	0.47
28 d	0.17	28 d	0.51	28 d	0.47	28 d	0.68
91 d	0.40	91 d	0.32	91 d	0.52	91 d	0.40

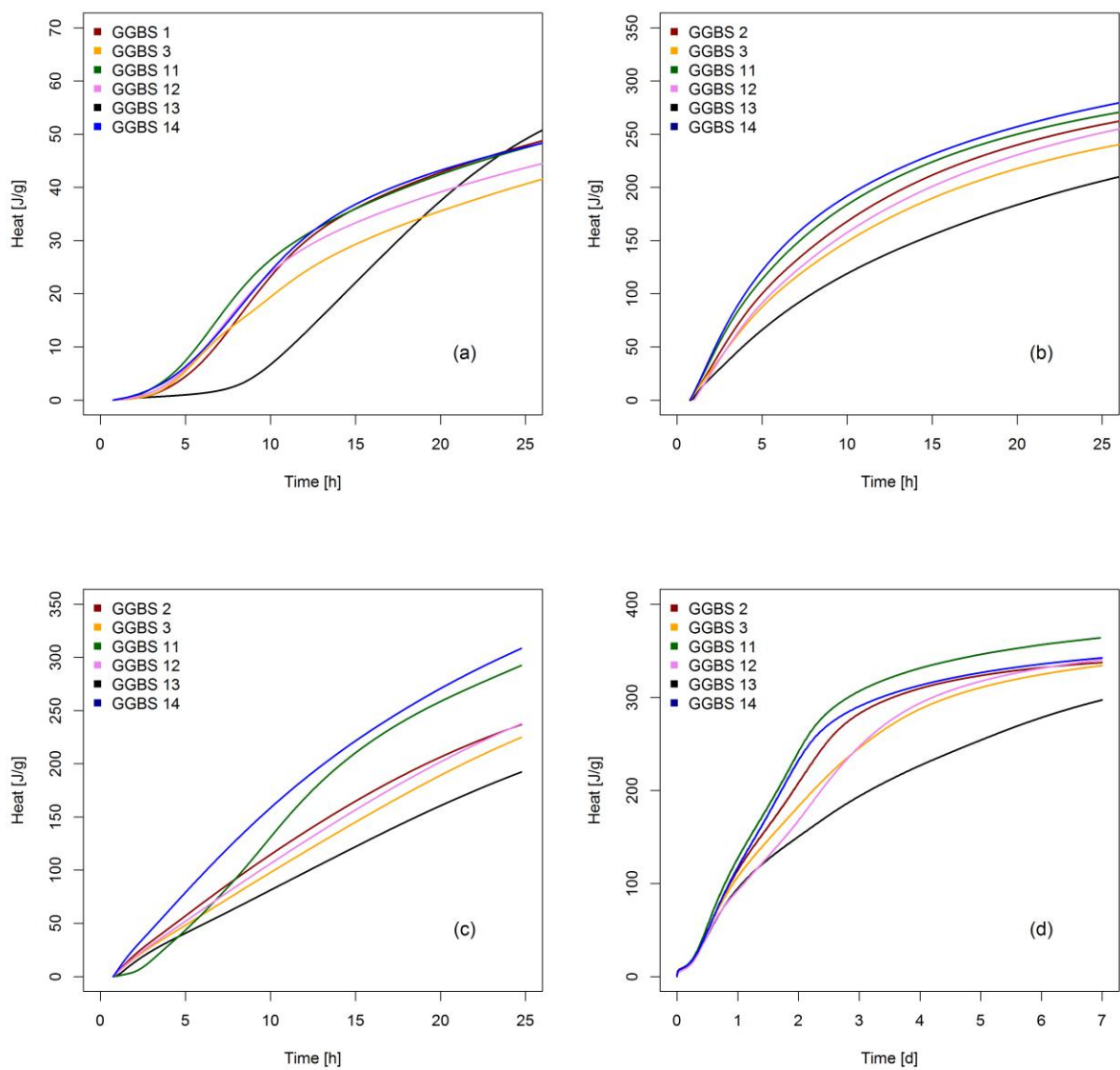
285

286 Linear regression of heat values against compressive strength for different ages, show similar
 287 patterns for the three rapid methods. Accuracy of fit is judged by Pearson’s R² for linear regressions
 288 (Table 6). The best fit is achieved for 2 d resistance values for the three model systems. The best
 289 correlation is calculated between the R3 test heat and 2 d compressive strength with an R² of 0.95,
 290 followed by the method taken from Snellings and Scrivener (2016) with an R² of 0.92. These R² values
 291 are similar to the correlation coefficients observed for calcined clay reactivity and 28d compressive
 292 strength of various SCMs [19,22]. Goodness of fit is progressively degrading towards higher and
 293 lower ages.

294 Only the method taken from Kashani et al. 2014 shows a better fit for 91 d old samples than for 28 d
295 and 7 d old samples [29]. Generally, fits are less accurate for the Kashani et al. 2014 method,
296 between 0.67 and 0.17. In the 7 d method adding clinker, the distribution of Pearson's R^2 values
297 differs from the model systems [29]. In this method, best fit is calculated for 28 d strength (0.68) and
298 2 d strength (0.59). Surprisingly, the correlation coefficient for 7 d compressive strength
299 corresponding to the calorimetric measurement time of 7 d is less well (0.47). However, the
300 correlation coefficient is never as high as for the methods at 40°C and Ca excess.

301 Heat curves of the Kashani et al. (2014) method (Figure 4) show different curve shapes for different
302 samples, with for example heat development of GGBS 13 starting after about 7 h and then starting to
303 overtake all other slags from 20 h on, also other heat curves intersect [29]. Also in the 7d test
304 method and the R3 test some sample change ranks during the test. This makes the cutoff time a
305 relevant parameter in the testing process. In literature, different cutoff times were proposed for the
306 R3 test. In Avet et al. (2016), 1 d measurements correlated well with compressive strength
307 development of blended cements containing calcined clays at all ages. Independent of SCM type it
308 was found that 3 d and 7 d heat release by the R3 test correlated well with 28 d compressive
309 strength of 30 % SCM blended cements, for various SCMs. 7 d compressive strength was well
310 correlated with all tested calorimetric cutoff times (0.5, 1, 3 and 7 d).

311 The R3-test was retained for further investigation for its large span of heat values, best correlation
312 with 2 d compressive strength results and its easier sample handling due to high water content.



313

314 **Figure 4. Isothermal calorimetry results applying the four different methods to 6 selected GGBS.**

315 **(a) Method described by Kashani et al. (2014)[29], (b) method by Snellings and Scrivener (2016)**

316 **[20], (c) R3 test described by Avet et al. (2016) and Li et al. (2018) [19,22] and (d) calorimetric test**

317 **using GGBS/clinker mixture (75:25) and sulfates according to EN 196-1 [31]. Note the different time**

318 **scale for (d). All heat measurements are normalized to slag mass in the vessel.**

319

320

321 **4.3.2 Method validation and sample preparation**

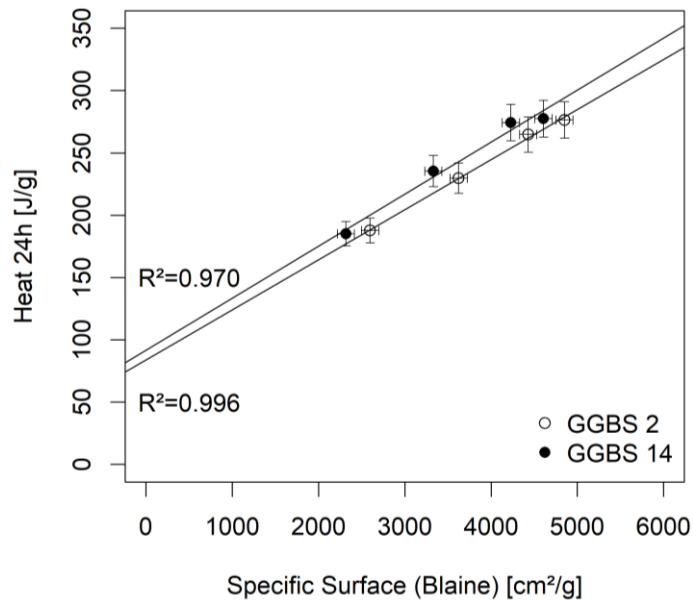
322 Validation of the R3 protocol showed good repeatability with a relative standard deviation of 0.87 %
 323 of the mean value (Table 7). The relative standard deviation of the same granulate ground 6 times
 324 had a relative standard deviation of 1.59 %.

325 **Table 7. Validation of the R3 protocol. The first sample set shows values measured on the same**
 326 **powder sample. In the second set grinding was included in the procedure.**

Sample type	Same Powder		Same granulate	
	Sample	Heat [J/g]	Sample	Heat [J/g]
	GBS 11.1	294.05	GGBS 14.1	264.17
	GBS 11.2	292.76	GGBS 14.2	264.37
	GBS 11.3	299.53	GGBS 14.3	263.53
	GBS 11.4	297.52	GGBS 14.4	271.33
	GBS 11.5	293.86	GGBS 14.5	258.98
	GBS 11.6	292.91	GGBS 14.6	261.12
	GBS 11.7	294.04		
Mean	[J/g]	294.95		263.92
SD	[J/g]	2.56		4.18
Relative SD	[%]	0.87		1.59

327

328 Measuring samples of different finesse point out the impact of specific surface on heat of hydration
 329 (Figure 5). The specific surface of the different samples was between 2500 ± 100 and 4800 ± 100
 330 cm^2/g , as determined by the Blaine method [32]. As expected, a higher reaction heat was measured
 331 when the samples were finer. Linear regression of reaction heat on Blaine value gave R^2 values >
 332 0.95, thus proportionality can be assumed. Applying the regression function suggests, that reaction
 333 heat increased by about 4 J/g for each $100 \text{ cm}^2/\text{g}$ increase of reactive surface.



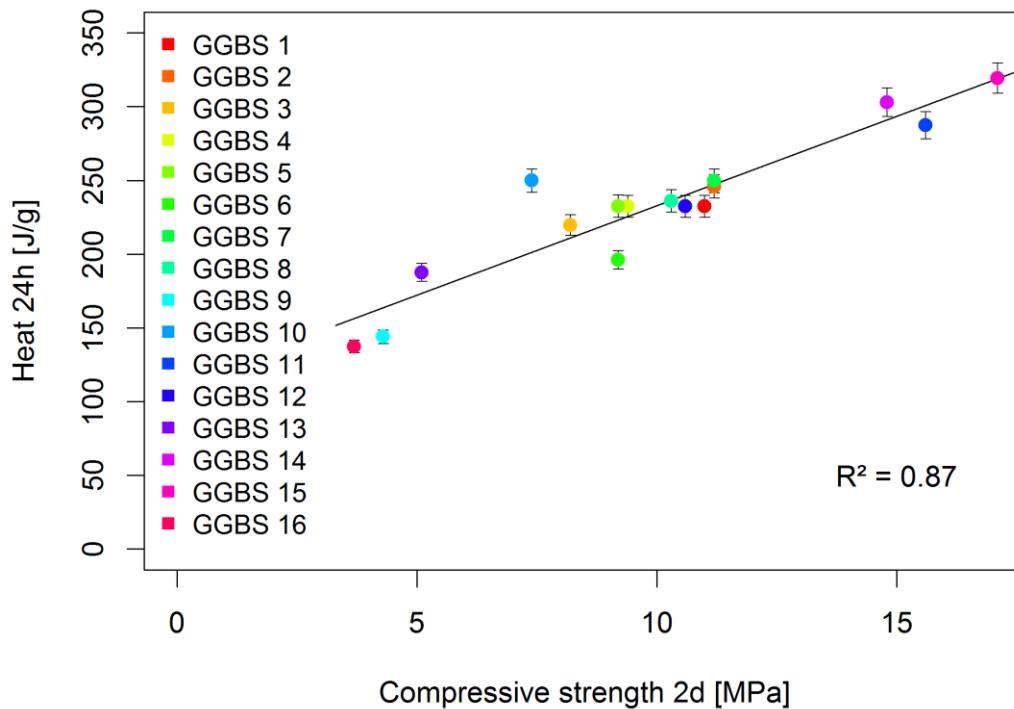
334

335 **Figure 5. Heat of hydration of GGBS 2 and GGBS 14 samples ground to different specific surface**
 336 **values, using the modified R3 protocol. Vertical error bars correspond to 2RSD intervals as**
 337 **described above. Horizontal error bars correspond to an average error of ± 100 cm²/g for the Blaine**
 338 **method.**

339

340 **4.3.3 Application of the R3-test on the set of 16 industrial GGBS**

341 In a last step all industrial slag samples were measured using the retained, R3 protocol. GGBS 9 was
 342 the industrial slag with lowest heat development (144 J/g), whereas GGBS 15 showed highest
 343 reaction heat with 319 J/g. The heat development for the 16 slag samples correlates well with mortar
 344 compressive strength after 2 days (Table 4), as linear regression gave a R^2 of 0.87 (Figure 6). This
 345 correlation coefficient is higher than for any reactivity index. The method error was estimated to be
 346 3.2 % using the 2 RSD interval computed from the validation trial reported in Table 6. Taking into
 347 account this error, not all slags can be separated from each other but there is a clear tendency for
 348 higher heat values in more reactive slags.



349

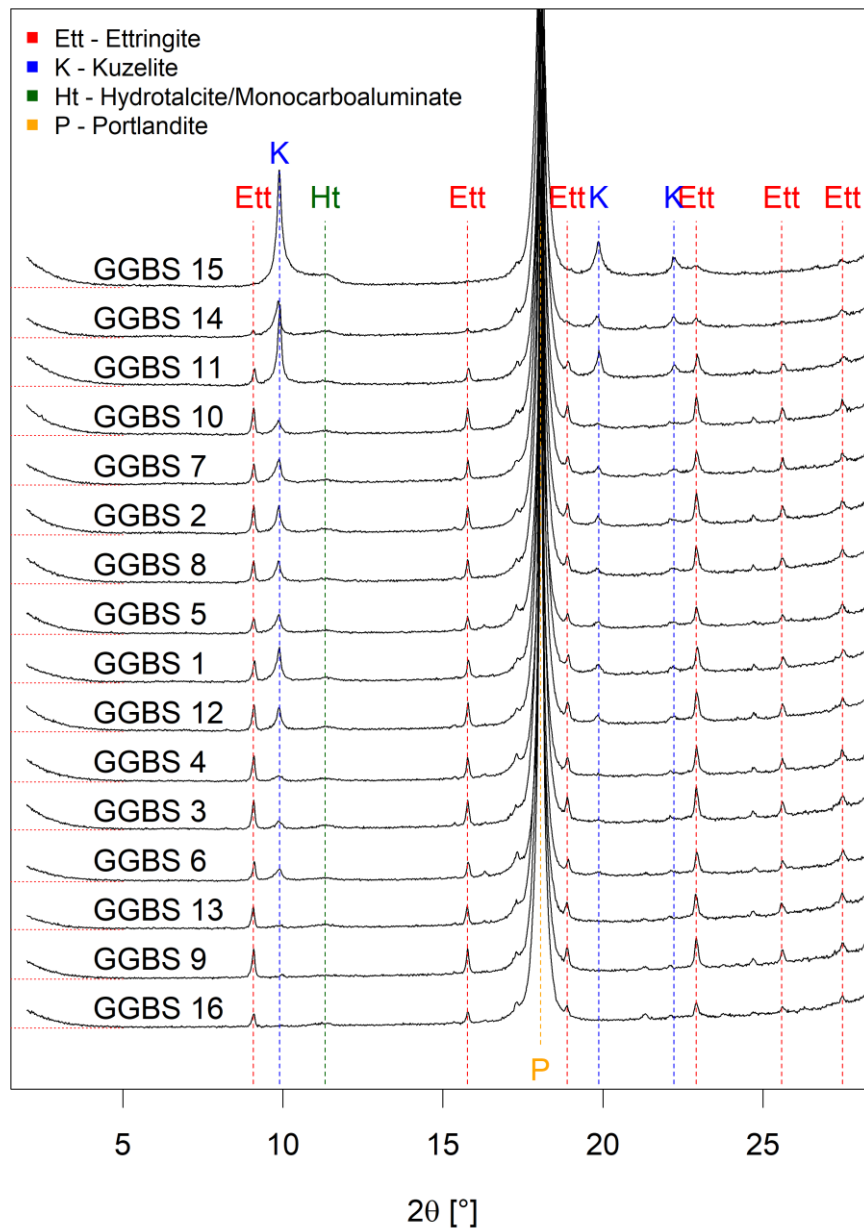
350 **Figure 6. Heat of hydration of the whole set of 16 GGBS, plotted against 2d compressive strength**
 351 **test results. Vertical error bars correspond to 2RSD intervals as described above.**

352

353 **4.4 Characterization of hydrates after calorimetric test**

354 After 24 h reaction time portlandite is still the major mineral phase in all samples as can be seen from
 355 the intense reflection at 18° in Figure 7. Besides, similar crystalline (ettringite, kuzelite) and
 356 amorphous phases (hydrotalcite) can be identified on XRD spectra in all slags after running the R3
 357 calorimetric measurements (Figure 7). However, marked differences exist in peak intensity. The
 358 kuzelite peaks are more intense in the most reactive slags, whereas ettringite peaks are virtually
 359 absent in those GGBS. In moderately reactive slags kuzelite, a monosulphate ($\text{Ca}_4\text{Al}_2(\text{SO}_4)(\text{OH})_{12} \cdot 6$
 360 H_2O) and ettringite ($\text{Ca}_6\text{Al}_2(\text{SO}_4)_3(\text{OH})_{12} \cdot 26 \text{H}_2\text{O}$) peaks coexist, whereas ettringite peaks are much
 361 more pronounced in least reactive slags. A broad hydrotalcite peak is visible in all slags, but most
 362 pronounced in the most reactive slag GGBS 15. The broad peak shape is likely due to variable
 363 compositions and especially in Mg/Al ratios of hydrotalcite. Also, hydrotalcite peaks overlap with

364 those of monocarboaluminates. Even though source of carbonates are limited in our setting, both
365 phases might be present.



366

367 **Figure 7. XRD patterns of pastes hydrated for 24 h using R3 protocol. The slags are ordered**
368 **according to their 24h heat development (GBS 15 being the highest and GGBS 16 the least reactive**
369 **slag).**

370

372 **5. Discussion**

373 **5.1 Differences in performance between different GGBS**

374 Important differences in strength development were observed for the different slags. Compressive
375 strength results at different hydration ages can differ by as much as a factor 4 between different
376 slags (Table 4). The highest dispersion of compressive strength is observed for the 2 d time step,
377 indicating a maximal influence of GGBS properties on compressive strength at this age. The highest
378 dispersion and largest span make the 2 d time step the most relevant for reactivity testing, besides
379 the practical interest in a short-term reactivity test.

380 At earlier ages, a major influence of clinker added is expected, due to its higher reaction rate [36]. At
381 later ages, compressive strength values of different GGBS samples converge. In literature GGBS
382 blended cements are known for ongoing hydration processes for long periods of time, also
383 differences in reaction degree were still visible after 1 year [37]. This is consistent with the
384 observation that strength development goes on until 91 d in our study, furthermore hierarchy
385 between most and least reactive slags stay the same indicating that some influence of GGBS
386 composition is still visible.

387 The exception is GGBS 15 with an extreme Al_2O_3 content. This sample shows the highest
388 compressive strength at 2 d but performs less well at later ages (Table 4). Similar behavior is known
389 for slags with high Al_2O_3 contents [9,10,38,39]. In blended cements, increased Al_2O_3 content of GGBS
390 was reported to enhance reaction heat and early age strength [37,38]. This is in contrast to results
391 obtained for alkali activated GGBS and activation systems using waterglass, where high Al_2O_3
392 contents had no or a negative effect on compressive strength [40,41]. In our case, the lower long-
393 term compressive strength of GGBS 15 appears to be due to the low CaO content (Table 1). The CaO
394 content of GGBS is reported to control short range order of C-S-H in alkali activated materials [42].

395 These observations underline the importance of Al-bearing phases for early age compressive
396 strength, and the importance of C-S-H phases for later strength development.

397 Several reactivity indices correlate well with early age strength, all of them use CaO and Al₂O₃ as
398 numerator (Table 5). Three of four also add MgO content as an asset. All divide by the SiO₂ content.
399 This homogeneity underlines that the first order influence of those elements on GGBS reactivity is
400 well understood. It is interesting to note that the index with the highest correlation with 2 d strength
401 $((C+A+M)/S)$ can be approximated as $(100-S)/S$, thus the reactivity can be resumed only by the SiO₂
402 content of the slag [9]. All indices perform less well at later ages, underlining that strength
403 development is less influenced by GGBS composition and reactivity at that stage. In the past
404 Smolczyk 1978, used the same linear regression approach on a set on 196 GGBS, his regressions on 2
405 d compressive strength in mortar systems gave lower R² values [10]. This is likely due to higher and
406 more stable glass contents and better control of minor elements in modern GGBS. Still, this
407 underlines the importance of composition for GGBS reactivity.

408 The mechanisms of influences of composition on GGBS reactivity are multiple. The chemical
409 composition of liquid slag exerts a control on the formation of the glass network. The higher the
410 content of network modifiers Mg, Ca, Na, K, the lower is the polymerization degree of the glass
411 network resulting in a less stable slag, showing higher dissolution rates [43,44]. Higher dissolution
412 rates imply a quicker liberation of ions to the liquid phase, which precipitate to give secondary
413 minerals that may develop material strength. The role of other elements in glass stability is less
414 clear, Al and Ti for example can act as both network formers and modifiers. NMR studies on GGBS
415 indicate mainly 4-coordinated Al, indicating rather a network former role of Al [38,45].

416 However, GGBS composition is not the only factor controlling glass structure. Also physical
417 parameters of the production process influence the glass structure, most importantly thermal
418 history, determined mainly by tapping temperature and quenching speed [1,11,14,15,46]. The
419 presence of different elements in the glass network also modifies the dissolution of the glass, the

420 presence of network forming Al, for example increases the dissolution rate, as Al-O-Si sites are more
421 easily attacked at high pH values than Si-O-Si groups [43]. In contrast, the insertion of other network
422 formers like Zr slows down dissolution rates [47].

423 Chemical composition of GGBS also controls the element release into solution, as a congruent slag
424 dissolution is expected [48,49]. Different stoichiometric ratios of elements can cause the formation
425 of different secondary phases, as was observed in literature by XRD, SEM, DTG techniques and
426 thermodynamic modelling of hydrated blended cements, and confirmed by XRD in this study [37].
427 For example MgO is essential for the formation of hydrotalcite like phases, and its formation lowers
428 the uptake of Al in C-A-S-H phases [39,50]. Also, in alkali activated binders higher MgO content was
429 found to increase reactivity (Ben Haha et al., 2011) [50]. Durdzinski et al. (2017) argue that the type
430 of hydrates is not important for strength development in blended cements and that the key factor is
431 space filling [51]. In contrast, Thermkhajorkit et al. 2014 found that in OPC pastes C-S-H phases are
432 more important in compressive strength development than other hydrates [52].

433 The multitude of mechanisms by that GGBS composition influence its reactivity make clear that a
434 prediction of reactivity only based on differences in composition is complex. Even though,
435 differences in composition might be the reason for differences in reactivity. Furthermore structural
436 and physical properties of the slag are neglected, calling for a more integrative method for evaluating
437 reactivity [9].

438

439 **5.2 Probing into reactivity using isothermal calorimetry**

440 In the first test using 6 selected GGBS, the two protocols using Ca(OH)₂ addition at 40°C showed the
441 best correlation with 2 d compressive strength values (Table 6). We chose the R3 method based on
442 Avet et al., (2016) and Li et al., (2018) for further investigation as sample handling was much easier

443 due to higher l/s ratio and for higher absolute heat values and larger relative differences between
444 samples [19,22].

445 Applied to the set of 16 industrial GGBS, the R3 test gives better correlation with 2 d compressive
446 strength ($R^2=0.87$) in a 75 wt.-% GGBS 25 wt.-% clinker system, than any of the reactivity indices
447 (Figure 6). Similar reaction pathways in the different samples can be assumed as heat curve shapes
448 are similar, only GGBS 11 shows a latency phase (Figure 4). The R3 test thus gives an intrinsic
449 reactivity of a given GGBS. This is especially interesting, as for the test no cement was used and thus
450 it gives comparable results of GGBS reactivity, without bias associated to the use of cement whose
451 composition might vary over time and with geographical origin. At later ages the test results
452 correlate less with compressive strength values, this in contrast to results obtained when calcined
453 clays were tested and heat release correlated well at all ages [22]. The test method, taken from
454 Snellings and Scrivener (2016), that also adds $\text{Ca}(\text{OH})_2$ in excess, performed only slightly less well. The
455 similarity between the results indicate that Ca excess is crucial for the performance of the
456 calorimetric test. Li et al. (2019) reported that longer calorimetric measurement times (3d, 7d)
457 correlated well with 28 d compressive strength in a large variety of SCMs. In this study, however,
458 measurement of these time steps was not attempted.

459 The R3 test showed a high sensibility to sample finesse. When the test was performed on samples
460 ground to different finesses in the range of 2500 to 5000 cm^2/g the reaction heat increased
461 proportional to sample fineness (Figure 5). Applying the regression equation shows that in our case
462 heat release increases by about 4 J/g with every additional 100 cm^2/g of fineness. This is a great
463 advantage over chemical reactivity indices, as the important physical reactivity parameter – fineness,
464 is included in the measurement. On the other hand, when differences due to sample compositions
465 are to be assessed, one needs to take care to control for sample fineness. Superposing PSD curves
466 (Figure 3) of the 16 GGBS used in this study suggest that it is sufficient to apply the same grinding
467 protocol to obtain similar PSD in a wide range of GGBS. However, during method validation the RSD

468 between replicates increased to 1.59 % when grinding was included in the procedure (Table 7). When
469 only the calorimetric protocol was repeated, the RSD was 0.87 %. This illustrates that the calorimetric
470 protocol of the R3 test is repeatable and very sensitive even to slight changes in PSD.

471 The calorimetric test proposed by Kasahni et al., (2014) did not correlate as well with compressive
472 strength, in the set of 6 GGBS [29]. This is likely due to the absence of a supplementary Ca-source in
473 this test. It still showed highest correlation with compressive strength at 2 d ($R^2 = 0.67$). Different
474 heat curve shapes indicate that the reaction mechanisms differed between different samples. This
475 led to different rankings of GGBS at different time steps. It is interesting to note the high
476 performance of GGBS 13 in this test. In the other tests, GGBS 13 was the least reactive slag. This
477 finding indicates, that different GGBS might show different reactivities in different activation
478 systems. This means that a badly performing GGBS with one system might show higher reactivity
479 with another activation system. The differences in heat development indicate that GGBS
480 composition has an impact on reactivity also in purely alkali activated systems. This is in contrast to
481 earlier studies by Ben Haha et al., (2011 and 2012), yet we do not provide data on compressive
482 strength of alkali activated materials [40,50].

483 Calorimetric measurements over 7 d, using the same clinker as the compressive strength test
484 correlated less well with compressive strength results, than the formerly mentioned test at any time.
485 It is especially interesting to note that also the 7 d compressive strength results, corresponding to the
486 duration of the calorimetric measurements, only showed weak correlation with released heat.

487

488 **5.3 Microstructure of samples and reaction mechanisms during the R3 test**

489 XRD scans after the R3-test show similar phase assemblages in all samples. The detected phases are
490 typically found in binders with high GGBS content, even though no cement was added [37]. However,
491 Ca is supplied by portlandite excess and the concentrations of SO_4 and K mainly come from the

492 solution and are thus the same in all samples. There appears to be a systematic difference in
493 ettringite and AFm phases close to kuzelite structure. The XRD scans from least reactive GGBS show
494 no kuzelite peak, but a clearly distinguishable ettringite peak (Figure 7). For more reactive GGBS an
495 AFm peak close to kuzelite structure appears and its intensity overtakes that of ettringite for the
496 most reactive samples. In GGBS 15, the most reactive GGBS, no ettringite is detected. It is likely that
497 the higher Al content of the more reactive GGBS causes this shift, as a main difference between
498 those minerals is the Al/Ca ratio, with kuzelite containing more Al with respect to Ca, than ettringite.
499 This is consistent with former research showing that composition of hydrates can be modified by
500 GGBS compositions and high Al contents are good for early age strength development of GGBS [37].
501 The early strength development due to higher Al contents is often associated with voluminous
502 ettringite formation, this is not confirmed here [40,53]. Also, hydrotalcite appears to be more
503 abundant in the most reactive samples. Liberation of MgO from the GGBS is essential for the
504 formation of hydrotalcite like phases, and its formation lowers the uptake of Al in C-A-S-H phases
505 [39,50]. In alkali activated GGBS presence of hydrotalcite led to higher long-term compressive
506 strength due to reduced coarse pore volume [50]. Consequently, the formation of hydrotalcite
507 appears to be a desirable feature also in blends adding OPC or portlandite.

508 The importance of Al bearing hydrates for early age strength development might also be the reason
509 for the sensitivity of the R3-test to early age reactivity. Formation of Al bearing phases is very
510 exothermic, compared to the formation of C-S-H phases that are responsible for later age strength
511 [54]. Ettringite for example has a formation enthalpy of $-17,535$ kJ/mol under standard conditions,
512 whereas formation enthalpy of tobermorite is given with $-1,916$ kJ/mol, almost ten times less [54]. It
513 was argued that differences in hydration enthalpy are due to differences in the amount of water
514 integrated to the crystal structure [55]. Ettringite and AFm phase take up more water to their
515 structure than CSH phases and have higher molar volume [54,55]. The higher molar volume might
516 explain their importance in early age strength as these phases can rapidly fill up pore space. The
517 differences in formation enthalpies and molar volume could be the reason why the 7 d calorimetric

518 test does not correlate well with 7 d compressive strength. At this age, strength development might
519 not be controlled by the same phases that control heat release. A calorimetric test can only work
520 when both coincide, which appears to be the case for early age, in blended cements that contain
521 high proportions of GGBS.

522 **6. Conclusion**

- 523 1. Large difference in slag reactivity exist, those are mainly but not exclusively due to
524 differences in GGBS composition. The influence is either due to dissolution rate of the glass
525 or type and structure of hydrates formed.
- 526 2. Differences in 2 d strength of blended cement pastes can be conveniently predicted by the
527 R3 method. The method does not work as well for later ages.
- 528 3. The R3 test proved to be highly sensitive to differences in fineness. Higher reactive surface
529 yield higher reaction heat at a rate of approximately 4 J/g per 100 cm². This is a great
530 advantage over reactivity indices.
- 531 4. Differences in compressive strength between GGBS in cements with high replacement rates
532 are most pronounced at early age, most notably 2 d in the studied systems. This is likely due
533 to the importance of Al bearing phases for early age strength.

534

535

536 **Acknowledgements**

537 This project has received funding from the Research Fund for Coal and Steel under grant agreement
538 No 749809.

539

- 541 [1] W. Matthes, A. Vollpracht, Y. Villagrán, S. Kamali-Bernard, D. Hooton, E. Gruyaert, M. Soutsos,
542 N. De Belie, Ground Granulated Blast-Furnace Slag, in: N. De Belie, M. Soutsos, E. Gruyaert
543 (Eds.), Prop. Fresh Hardened Concr. Contain. Suppl. Cem. Mater., Springer International
544 Publishing, Cham, 2018: pp. 1–53. https://doi.org/10.1007/978-3-319-70606-1_1.
- 545 [2] J. Bijen, Benefits of slag and fly ash, *Constr. Build. Mater.* 10 (1996) 309–314.
546 [https://doi.org/10.1016/0950-0618\(95\)00014-3](https://doi.org/10.1016/0950-0618(95)00014-3).
- 547 [3] A. Ehrenberg, CO₂ emissions and energy consumption of granulated blastfurnace slag, in: *Proc.*
548 *Manuf. Process. Iron Steel Slags*, Euroslag publication, Keyworth, UK, 2002: pp. 151–166.
- 549 [4] F. Hogan, J. Meusel, Evaluation for Durability and Strength Development of a Ground
550 Granulated Blast Furnace Slag, *Cem. Concr. Aggreg.* 3 (1981) 40.
551 <https://doi.org/10.1520/CCA10201J>.
- 552 [5] H.F.W. Taylor, *Cement chemistry*, 2nd ed., Thomas Telford Publishing, 1997.
553 <https://doi.org/10.1680/cc.25929>.
- 554 [6] P. Van den Heede, N. De Belie, Environmental impact and life cycle assessment (LCA) of
555 traditional and ‘green’ concretes: Literature review and theoretical calculations, *Cem. Concr.*
556 *Compos.* 34 (2012) 431–442. <https://doi.org/10.1016/j.cemconcomp.2012.01.004>.
- 557 [7] A. Ehrenberg, D. Israel, A. Kühn, HM. Ludwig, V. Tigges, W. Wassing, Hüttensand:
558 Reaktionspotenzial und Herstellung optimierter Zemente Tl.1 (Granulated blast furnace slag:
559 reaction potential and production of optimized cements, part 1), *Cem. Int.* (2008).
- 560 [8] N. Robeyst, E. Gruyaert, C.U. Grosse, N. De Belie, Monitoring the setting of concrete containing
561 blast-furnace slag by measuring the ultrasonic p-wave velocity, *Cem. Concr. Res.* 38 (2008)
562 1169–1176. <https://doi.org/10.1016/j.cemconres.2008.04.006>.
- 563 [9] H.-G. Smolczyk, Structure des laitiers et hydratation des ciments de laitiers : structure et
564 caractérisation des laitiers, in: *Rapp. PRINCIPAUX*, Paris, 1980: pp. III-1/1-1/17.
- 565 [10] H.-G. Smolczyk, Zum Einfluß der Chemie des Hüttensands auf die Festigkeit von
566 Hochofenzementen, *Zem. - Kalk - Gips.* (1978) 294–296.
- 567 [11] N. Pronina, S. Krüger, H. Bornhöft, J. Deubener, A. Ehrenberg, Cooling history of a wet-
568 granulated blast furnace slag (GBS), *J. Non-Cryst. Solids.* 499 (2018) 344–349.
569 <https://doi.org/10.1016/j.jnoncrysol.2018.07.054>.
- 570 [12] F. Schröder, Slags and slag cements, in: *Proc. 5th Int. Symp. Chem. Cem.*, Tokyo, 1969: pp. 149–
571 199.
- 572 [13] R. Tänzer, A. Buchwald, D. Stephan, Effect of slag chemistry on the hydration of alkali-activated
573 blast-furnace slag, *Mater. Struct.* 48 (2015) 629–641. <https://doi.org/10.1617/s11527-014-0461-x>.
- 574
- 575 [14] A. Ehrenberg, Influence of the granulation conditions and performance potential of granulated
576 blast-furnace slag – Part 1: Granulation conditions, *ZKG Int.* (2013) 64–71.
- 577 [15] A. Ehrenberg, Influence of the granulation conditions and -performance potential of granulated
578 blastfurnace slag – Part 2: Chemistry and physical properties, *ZKG Int.* (2013) 60–67.
- 579 [16] F. Bellmann, J. Stark, Activation of blast furnace slag by a new method, *Cem. Concr. Res.* 39
580 (2009) 644–650. <https://doi.org/10.1016/j.cemconres.2009.05.012>.
- 581 [17] K. Riding, D.A. Silva, K. Scrivener, Early age strength enhancement of blended cement systems
582 by CaCl₂ and diethanol-isopropanolamine, *Cem. Concr. Res.* 40 (2010) 935–946.
583 <https://doi.org/10.1016/j.cemconres.2010.01.008>.
- 584 [18] L. Steger, C. Patapy, B. Salesses, M. Chaouche, M. Cyr, Acceleration of GGBS Cements by
585 Chloride, *New Insights on Early Hydration*, (2017).
- 586 [19] X. Li, R. Snellings, M. Antoni, N.M. Alderete, M. Ben Haha, S. Bishnoi, Ö. Cizer, M. Cyr, K. De
587 Weerd, Y. Dhandapani, J. Duchesne, J. Haufe, D. Hooton, M. Juenger, S. Kamali-Bernard, S.
588 Kramar, M. Marroccoli, A.M. Joseph, A. Parashar, C. Patapy, J.L. Provis, S. Sabio, M. Santhanam,
589 L. Steger, T. Sui, A. Telesca, A. Vollpracht, F. Vargas, B. Walkley, F. Winnefeld, G. Ye, M. Zajac, S.

- 590 Zhang, K.L. Scrivener, Reactivity tests for supplementary cementitious materials: RILEM TC 267-
591 TRM phase 1, *Mater. Struct.* 51 (2018). <https://doi.org/10.1617/s11527-018-1269-x>.
- 592 [20] R. Snellings, K.L. Scrivener, Rapid screening tests for supplementary cementitious materials:
593 past and future, *Mater. Struct.* 49 (2016) 3265–3279. [https://doi.org/10.1617/s11527-015-](https://doi.org/10.1617/s11527-015-0718-z)
594 0718-z.
- 595 [21] V. Kocaba, E. Gallucci, K.L. Scrivener, Methods for determination of degree of reaction of slag in
596 blended cement pastes, *Cem. Concr. Res.* 42 (2012) 511–525.
597 <https://doi.org/10.1016/j.cemconres.2011.11.010>.
- 598 [22] F. Avet, R. Snellings, A. Alujas Diaz, M. Ben Haha, K. Scrivener, Development of a new rapid,
599 relevant and reliable (R3) test method to evaluate the pozzolanic reactivity of calcined kaolinitic
600 clays, *Cem. Concr. Res.* 85 (2016) 1–11. <https://doi.org/10.1016/j.cemconres.2016.02.015>.
- 601 [23] S.T. Erdoğan, T.Ç. Koçak, Influence of slag fineness on the strength and heat evolution of
602 multiple-clinker blended cements, *Constr. Build. Mater.* 155 (2017) 800–810.
603 <https://doi.org/10.1016/j.conbuildmat.2017.08.120>.
- 604 [24] K. Tang, J. Khatib, G. Beattie, Effect of partial replacement of cement with slag on the early-age
605 strength of concrete, *Proc. Inst. Civ. Eng. - Struct. Build.* 170 (2017) 451–461.
606 <https://doi.org/10.1680/jstbu.16.00038>.
- 607 [25] K. Tang, S. Millard, G. Beattie, Early-age heat development in GGBS concrete structures, *Proc.*
608 *Inst. Civ. Eng. - Struct. Build.* 168 (2015) 541–553. <https://doi.org/10.1680/stbu.14.00089>.
- 609 [26] S. Ramanathan, H. Moon, M. Croly, C.-W. Chung, P. Suraneni, Predicting the degree of reaction
610 of supplementary cementitious materials in cementitious pastes using a pozzolanic test, *Constr.*
611 *Build. Mater.* 204 (2019) 621–630. <https://doi.org/10.1016/j.conbuildmat.2019.01.173>.
- 612 [27] P. Suraneni, J. Weiss, Examining the pozzolanicity of supplementary cementitious materials
613 using isothermal calorimetry and thermogravimetric analysis, *Cem. Concr. Compos.* 83 (2017)
614 273–278. <https://doi.org/10.1016/j.cemconcomp.2017.07.009>.
- 615 [28] Y. Wang, P. Suraneni, Experimental methods to determine the feasibility of steel slags as
616 supplementary cementitious materials, *Constr. Build. Mater.* 204 (2019) 458–467.
617 <https://doi.org/10.1016/j.conbuildmat.2019.01.196>.
- 618 [29] A. Kashani, J.L. Provis, G.G. Qiao, J.S.J. van Deventer, The interrelationship between surface
619 chemistry and rheology in alkali activated slag paste, *Constr. Build. Mater.* 65 (2014) 583–591.
620 <https://doi.org/10.1016/j.conbuildmat.2014.04.127>.
- 621 [30] P. Drissen, Determination of the glass content in granulated blast furnace slag., *Zem. - Kalk -*
622 *Gips.* (1994) 658–661.
- 623 [31] EN 196-1, Methods of testing cement - Part 1: Determination of strengt, n.d.
- 624 [32] EN 196-6, Methods of testing cement – Part 6: Determination of fineness, n.d.
- 625 [33] EN 196-9, Methods of testing cement – Part 9: Heat of hydration, Semi-adiabatic method, n.d.
- 626 [34] A. Ehrenberg, J. Deubener, N. Pronina, D. Hart, The glass structure of granulated blast furnace
627 slag and its effect on reactivity., in: *Proc. 15th Int. Congr. Chem. Cem.*, Prague, 2019.
- 628 [35] A. Ehrenberg, Granulated blast furnace slag - From laboratory into practice., in: Beijing, 2015.
- 629 [36] A. Schöler, B. Lothenbach, F. Winnefeld, M.B. Haha, M. Zajac, H.-M. Ludwig, Early hydration of
630 SCM-blended Portland cements: A pore solution and isothermal calorimetry study, *Cem. Concr.*
631 *Res.* 93 (2017) 71–82. <https://doi.org/10.1016/j.cemconres.2016.11.013>.
- 632 [37] M. Whittaker, M. Zajac, M. Ben Haha, F. Bullerjahn, L. Black, The role of the alumina content of
633 slag, plus the presence of additional sulfate on the hydration and microstructure of Portland
634 cement-slag blends, *Cem. Concr. Res.* 66 (2014) 91–101.
635 <https://doi.org/10.1016/j.cemconres.2014.07.018>.
- 636 [38] P.Z. Wang, R. Trettin, V. Rudert, T. Spaniol, Influence of Al₂O₃ content on hydraulic reactivity
637 of granulated blast-furnace slag, and the interaction between Al₂O₃ and CaO, *Adv. Cem. Res.*
638 16 (2004) 1–7. <https://doi.org/10.1680/adcr.2004.16.1.1>.
- 639 [39] W. Wassing, Relationship between the chemical reactivity of granulated blastfurnace slags and
640 the mortar standard compressive strength of the blastfurnace cements produced from them,
641 *Cem. Int.* (2003) 95–109.

- 642 [40] M. Ben Haha, B. Lothenbach, G. Le Saout, F. Winnefeld, Influence of slag chemistry on the
643 hydration of alkali-activated blast-furnace slag — Part II: Effect of Al₂O₃, *Cem. Concr. Res.* 42
644 (2012) 74–83. <https://doi.org/10.1016/j.cemconres.2011.08.005>.
- 645 [41] A.R. Sakulich, E. Anderson, C.L. Schauer, M.W. Barsoum, Influence of Si:Al ratio on the
646 microstructural and mechanical properties of a fine-limestone aggregate alkali-activated slag
647 concrete, *Mater. Struct.* 43 (2010) 1025–1035. <https://doi.org/10.1617/s11527-009-9563-2>.
- 648 [42] K. Gong, C.E. White, Impact of chemical variability of ground granulated blast-furnace slag on
649 the phase formation in alkali-activated slag pastes, *Cem. Concr. Res.* 89 (2016) 310–319.
650 <https://doi.org/10.1016/j.cemconres.2016.09.003>.
- 651 [43] B.C. Bunker, Molecular mechanisms for corrosion of silica and silicate glasses, *J. Non-Cryst.*
652 *Solids.* 179 (1994) 300–308. [https://doi.org/10.1016/0022-3093\(94\)90708-0](https://doi.org/10.1016/0022-3093(94)90708-0).
- 653 [44] H. Scholze, *Glass*, Springer New York, New York, NY, 1991. [https://doi.org/10.1007/978-1-4613-](https://doi.org/10.1007/978-1-4613-9069-5)
654 [9069-5](https://doi.org/10.1007/978-1-4613-9069-5).
- 655 [45] P.J. Schilling, L.G. Butler, A. Roy, H.C. Eaton, ²⁹Si and ²⁷Al MAS-NMR of NaOH-Activated Blast-
656 Furnace Slag, *J. Am. Ceram. Soc.* 77 (1994) 2363–2368. [https://doi.org/10.1111/j.1151-](https://doi.org/10.1111/j.1151-2916.1994.tb04606.x)
657 [2916.1994.tb04606.x](https://doi.org/10.1111/j.1151-2916.1994.tb04606.x).
- 658 [46] A. Ehrenberg, Granulated blast furnace slag - State of the art and potentials for the future CO₂
659 emissions and energy consumption of granulated blastfurnace slag, in: Euroslag publication,
660 Madrid, 2011: pp. 277–297.
- 661 [47] C. Cailleteau, F. Angeli, F. Devreux, S. Gin, J. Jestin, P. Jollivet, O. Spalla, Insight into silicate-glass
662 corrosion mechanisms, *Nat. Mater.* 7 (2008) 978.
- 663 [48] R. Snellings, Solution-Controlled Dissolution of Supplementary Cementitious Material Glasses at
664 pH 13: The Effect of Solution Composition on Glass Dissolution Rates, *J. Am. Ceram. Soc.* 96
665 (2013) 2467–2475. <https://doi.org/10.1111/jace.12480>.
- 666 [49] R. Snellings, T. Paulhiac, K. Scrivener, The Effect of Mg on Slag Reactivity in Blended Cements,
667 *Waste Biomass Valorization.* 5 (2014) 369–383. <https://doi.org/10.1007/s12649-013-9273-4>.
- 668 [50] M. Ben Haha, B. Lothenbach, G. Le Saout, F. Winnefeld, Influence of slag chemistry on the
669 hydration of alkali-activated blast-furnace slag — Part I: Effect of MgO, *Cem. Concr. Res.* 41
670 (2011) 955–963. <https://doi.org/10.1016/j.cemconres.2011.05.002>.
- 671 [51] P.T. Durdziński, M. Ben Haha, M. Zajac, K.L. Scrivener, Phase assemblage of composite cements,
672 *Cem. Concr. Res.* 99 (2017) 172–182. <https://doi.org/10.1016/j.cemconres.2017.05.009>.
- 673 [52] P. Termkhajornkit, Q.H. Vu, R. Barbarulo, S. Daronnat, G. Chanvillard, Dependence of
674 compressive strength on phase assemblage in cement pastes: Beyond gel–space ratio —
675 Experimental evidence and micromechanical modeling, *Cem. Concr. Res.* 56 (2014) 1–11.
676 <https://doi.org/10.1016/j.cemconres.2013.10.007>.
- 677 [53] A. Gruskovnjak, B. Lothenbach, L. Holzer, R. Figi, F. Winnefeld, Hydration of alkali-activated slag:
678 comparison with ordinary Portland cement, *Adv. Cem. Res.* 18 (2006) 119–128.
679 <https://doi.org/10.1680/adcr.2006.18.3.119>.
- 680 [54] B. Lothenbach, D.A. Kulik, T. Matschei, M. Balonis, L. Baquerizo, B. Dilnesa, G.D. Miron, R.J.
681 Myers, Cemdata18: A chemical thermodynamic database for hydrated Portland cements and
682 alkali-activated materials, *Cem. Concr. Res.* 115 (2019) 472–506.
683 <https://doi.org/10.1016/j.cemconres.2018.04.018>.
- 684 [55] R. Snellings, X. Li, F. Avet, K. Scrivener, A Rapid, Robust, and Relevant (R3) Reactivity Test for
685 Supplementary Cementitious Materials, *ACI Mater. J.* 116 (2019).
686 <https://doi.org/10.14359/51716719>.
- 687